Supporting Information

Revelation of a Catalytic Calcium-Binding Site Elucidates Unusual Metal Dependence of a Human Apyrase

David W. Rooklin[1], Min Lu[2] and Yingkai Zhang[1]*

[1] Department of Chemistry, New York University, New York, NY 10003

[2]Public Health Research Institute Center, Department of Microbiology and Molecular Genetics, UMDNJ – New Jersey Medical School, Newark, NJ 07103

The following supporting information includes Tables S1-S2, Figures S1-S12, and the complete citation for references 10, 13, 24, 40, 78, and 79.

Res ID	Wat	Ca^{2+}
D44	>12	>12
D46	>12	>12
E98	1.6	1.2
D114	>12	5.9
E147	>12	<0
E216	>12	>12
E297	<0	0.9
E328	>12	<0

Table S1: Calculated pKa values for active site ionizable residues in the crystal structure, with crystal-assigned active site water and with catalytic calcium replacement. The GDP substrate and structural calcium are present for both calculations. Large basic or acidic shifts are shown in green or red, respectively.

Metal Ion	CN	%Total	Metal Ion	CN	%Total
Mg2+	4	9%	Mn2+	4	7%
	5	7%		5	7%
	6	79%		6	75%
	7	4%		7	7%
Ca2+	6	22%	Zn2+	4	42%
	7	25%		5	19%
	8	45%		6	35%
	9	5%		7	4%
	10	3%			

Table S2: Observed coordination numbers for various divalent cations with their relative percentages, a survey from the Protein Databank data, adapted from [Glusker J.P.; Katz A.K.; Bock C.W. *The Rigaku Journal* **1999**, *16*, 8.] Note the relative flexibility of the calcium coordination chemistry and the accessible higher coordination numbers.

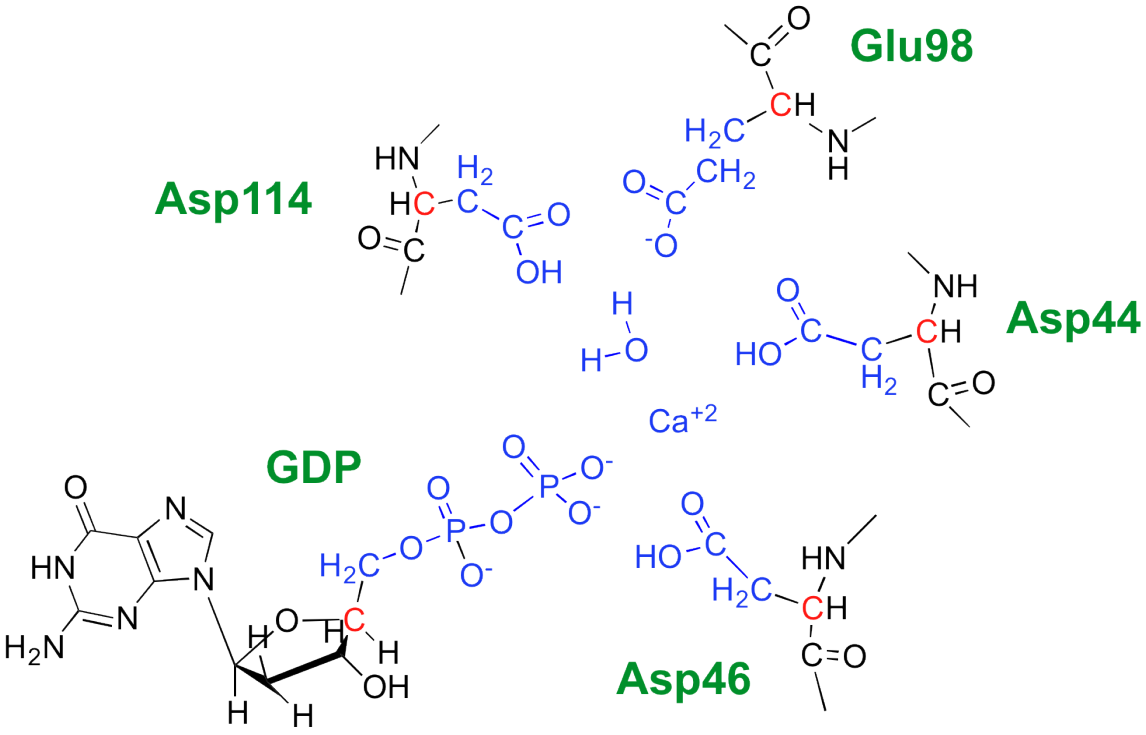

Figure S1. Depiction of the QM/MM partition scheme. Black, MM subsystem; Red, boundary carbon atoms in the QM subsystem described by improved pseudobond parameters; Blue, all other atoms in the QM sub-system.

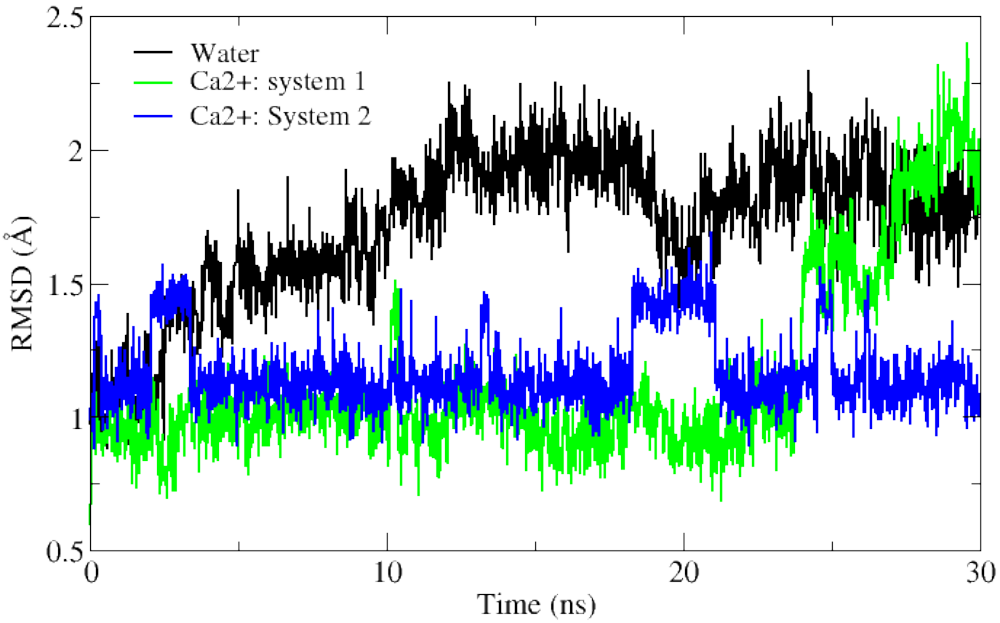

Figure S2. RMSD from the crystal coordinates for the side chain oxygens in the five residues that appear to interact with the proposed misassigned cationic atom: S100, D44, D114, E147, and E328. The colors correspond as follows, black: water, green: Ca^{2+} (with protonate E147 and E328—this is potentially the crystal structure state due to the acidic crystallization conditions), blue: Ca^{2+} (with deprotonated E147 and E328—this is our proposed reactant state).

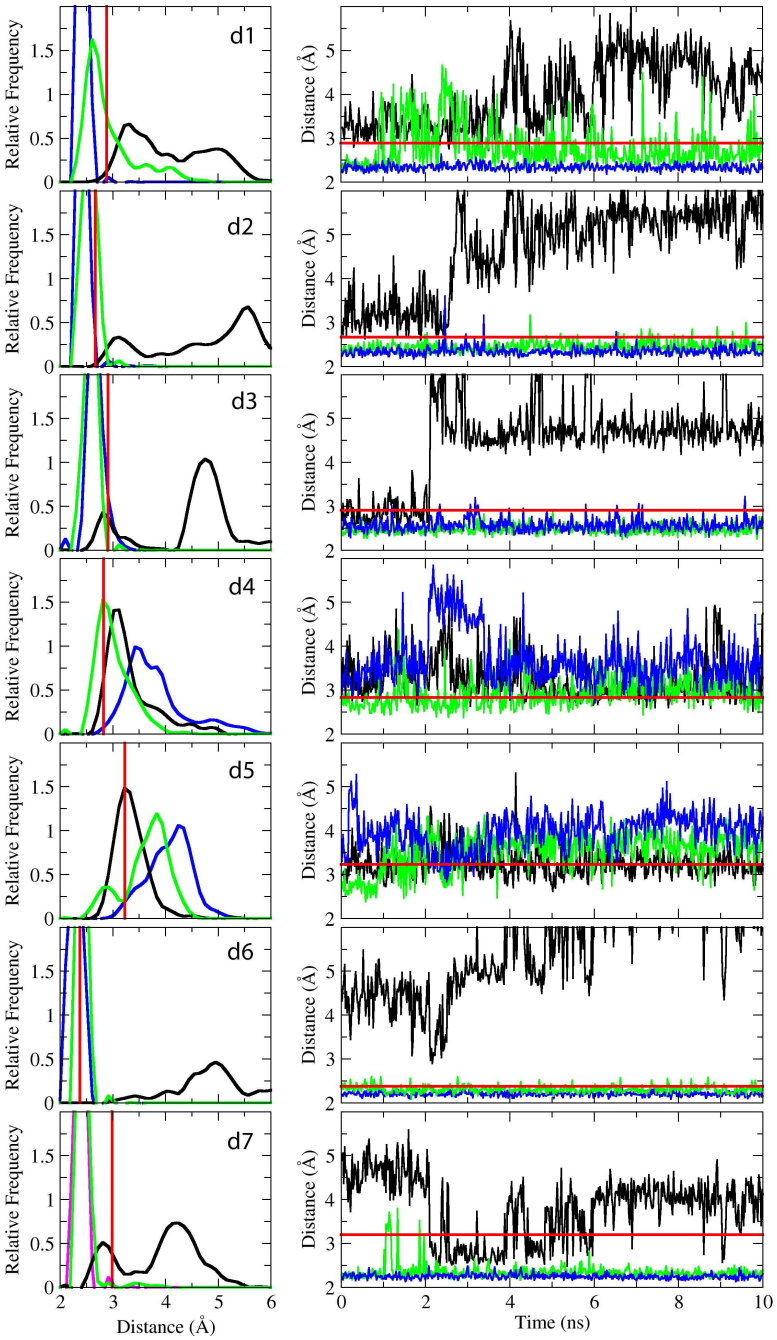

Figure S3. Time series and histograms for the 7 coordinated interactions from the first 10 ns of the MD trajectories, either with the crystal-assigned water or with calcium substitution. The colors correspond as follows, black: water, green: Ca^{2+} (with protonate E147 and E328—this is potentially the crystal structure state due to the acidic crystallization conditions), blue: Ca^{2+} (with deprotonated E147 and E328—this is our proposed reactant state). The values from the crystal structure are shown as red lines. The specific coordinated atoms are all oxygen atoms from the following residues, d1: E147, d2: E328, d3: S100, d4: D114, d5 D44, d6: alpha PHS, d7: beta PHS.

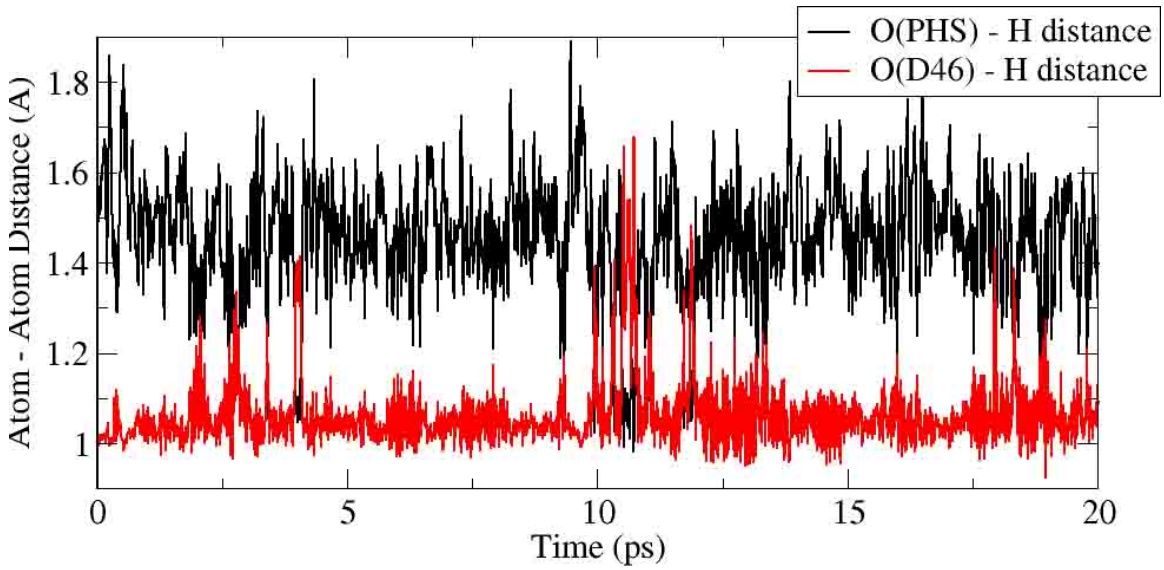

Figure S4. Time series of the two bond lengths involved in the low barrier hydrogen bond between D46 and the beta phosphate for a 20 ps unrestrained QM/MM MD trajectory. The multiple spontaneous crossings within 20ps indicate a low free energy barrier to this proton transfer.

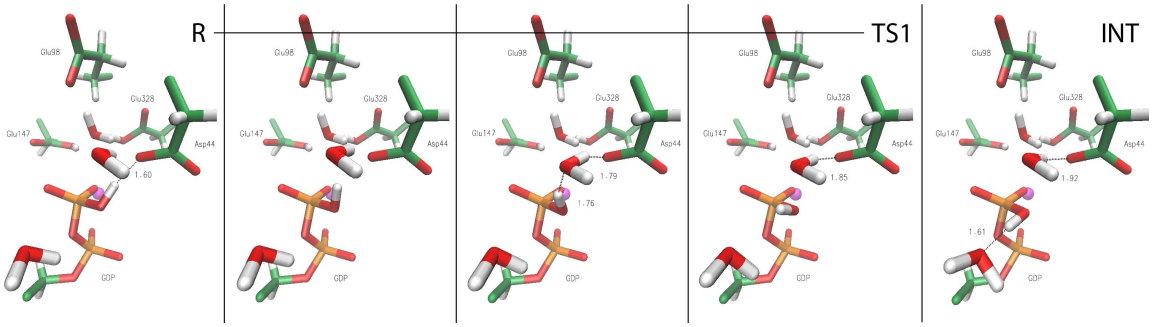

Figure S5. Structures across the dihedral rotation (step 1 of the suggested mechanism), from the reactant to the intermediate, depicting the stabilizing solvent interactions through the rotation.

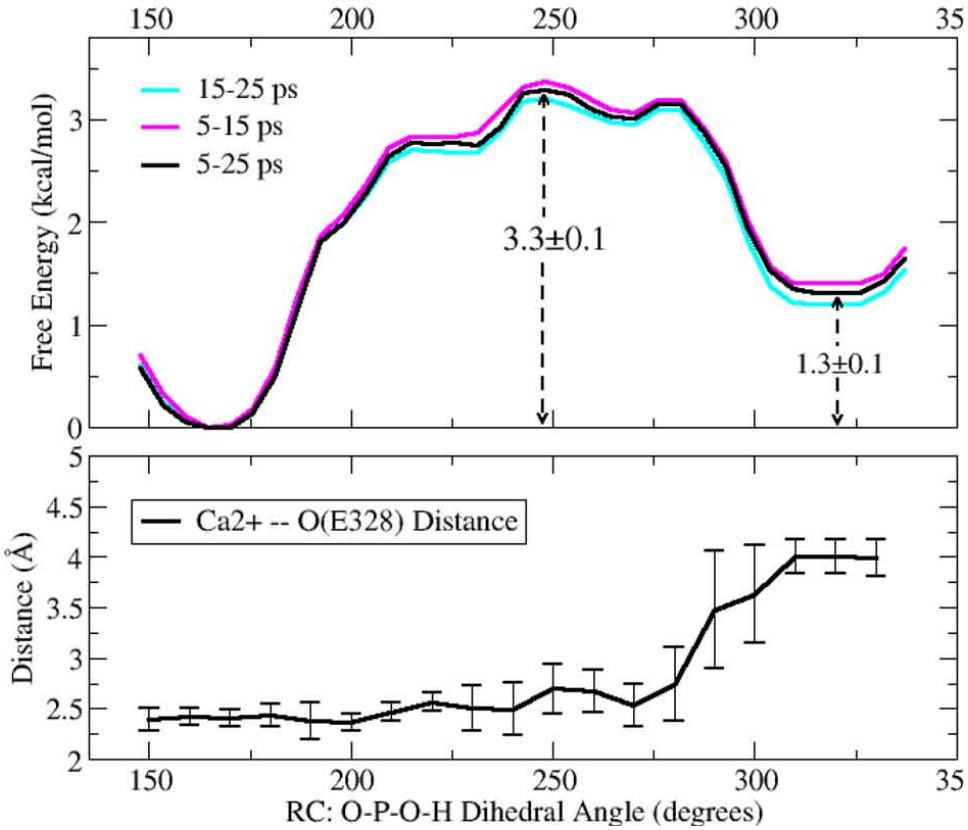

Figure S6. Top: Free energy profile for the dihedral rotation of the phosphoryl proton between D46, at 160˚ (the reactant state), and toward the leaving group, at 300˚ (the intermediate state). Bottom: Monitoring of the key Ca^{2+}-O(E328) interaction distance as the E328 coordination with the catalytic calcium shifts from bidentate to monodentate.

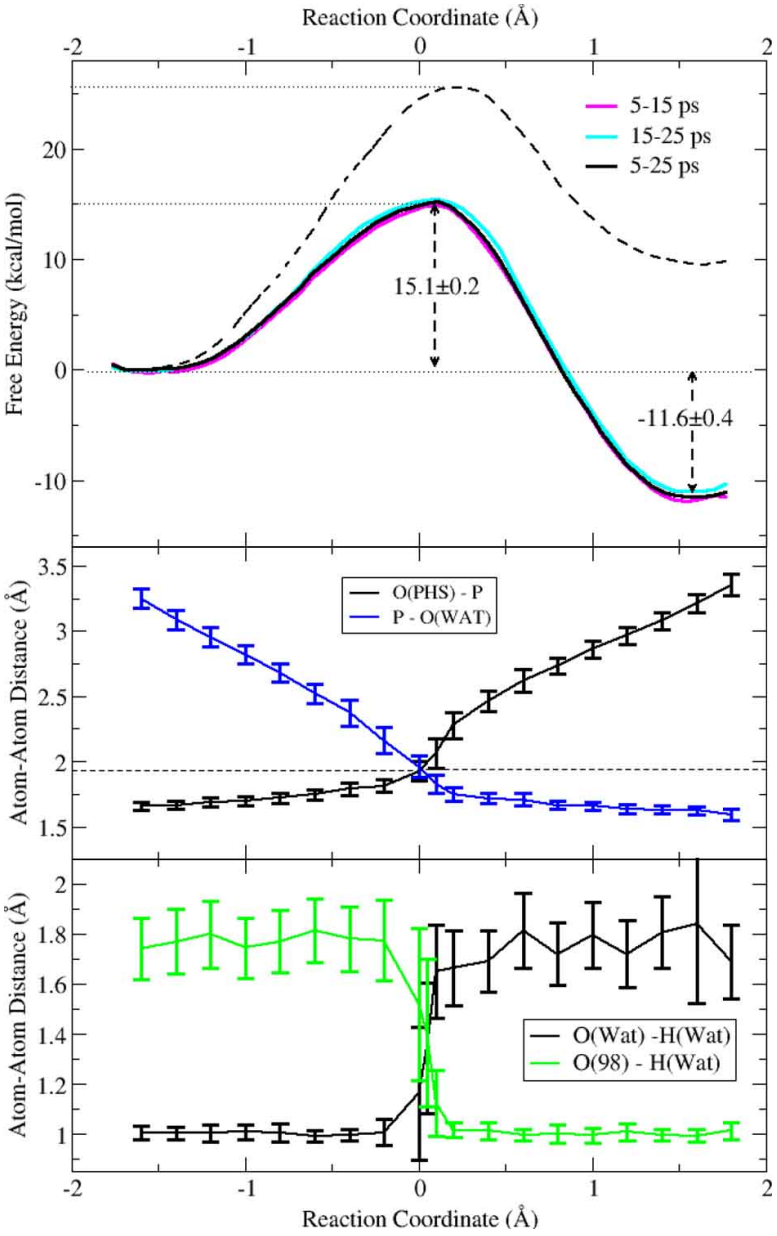

Figure S7. Top: Free energy profile for phosphoryl transfer starting at the intermediate, showing convergence within the 25 ps sampled per window. The dashed free energy profile is for the direct phosphoryl transfer from the reactant state (without the prior proton transfer from Asp46 and its rotation toward the leaving group), indicating the higher activation energy for the direct transfer. Middle: Distance averages and standard deviations for the two bonds in the *RC*, demonstrating adequate structural overlap between windows, and illustrating the concerted/synchronous mechanism. Bottom: Distance averages and standard deviations for the proton transfer from the nucleophile to the base E98, also showing adequate sampling.

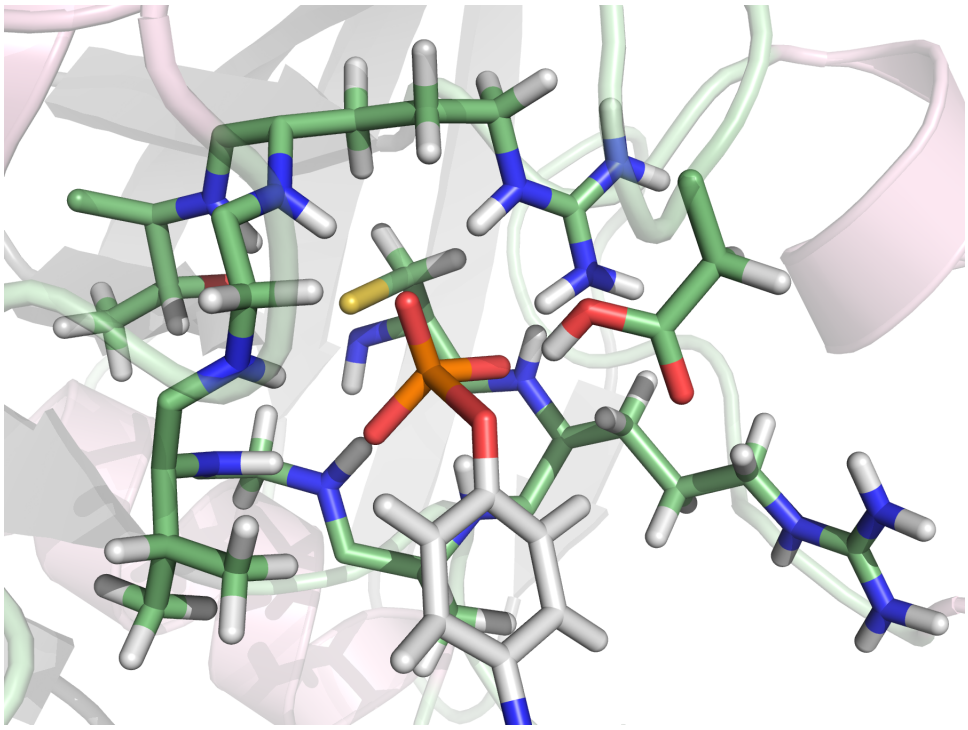

Figure S8: A representative P-loop/Walker A motif from the Yersinia PTP1B.[**Stuckey, J. A.; Schubert, H. L.; Fauman, E. B.; Zhang, Z. Y.; Dixon, J. E.; Saper, M. A.** ***Nature*** **1994,** ***370*****, 571.]** The backbone NH groups form an inward facing loop to favorably interact with the negative phosphate, here attached to tyrosine.

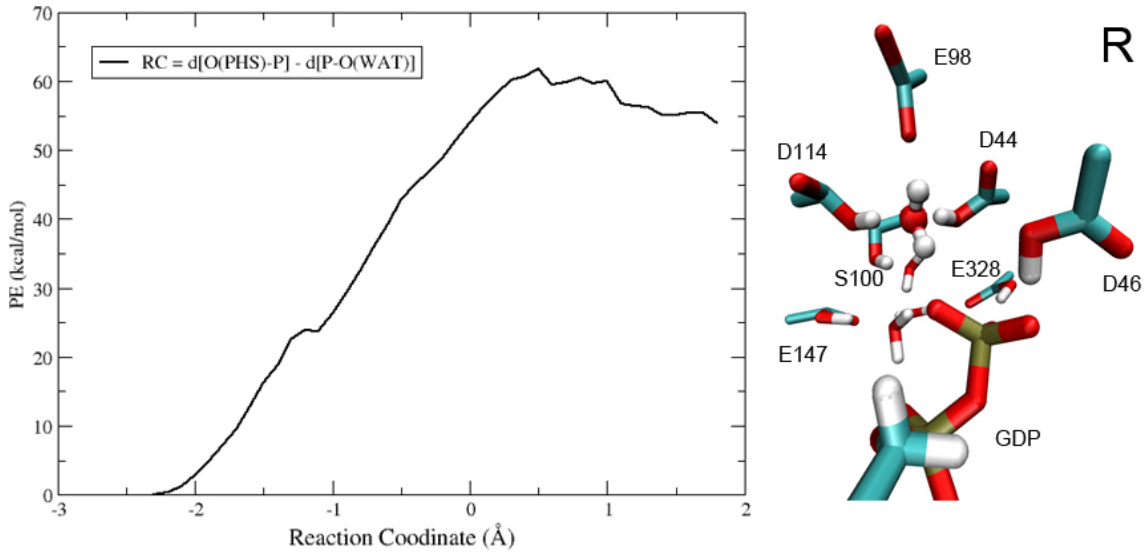

Figure S9. The potential energy barrier to phosphoryl transfer from the initial semi-stable system—with no catalytic calcium and the corresponding active site protonation state (Glu147 and Glu328 are protonated). The nucleophilic water is not optimally positioned in this system, and the activation energy is unreasonably high.

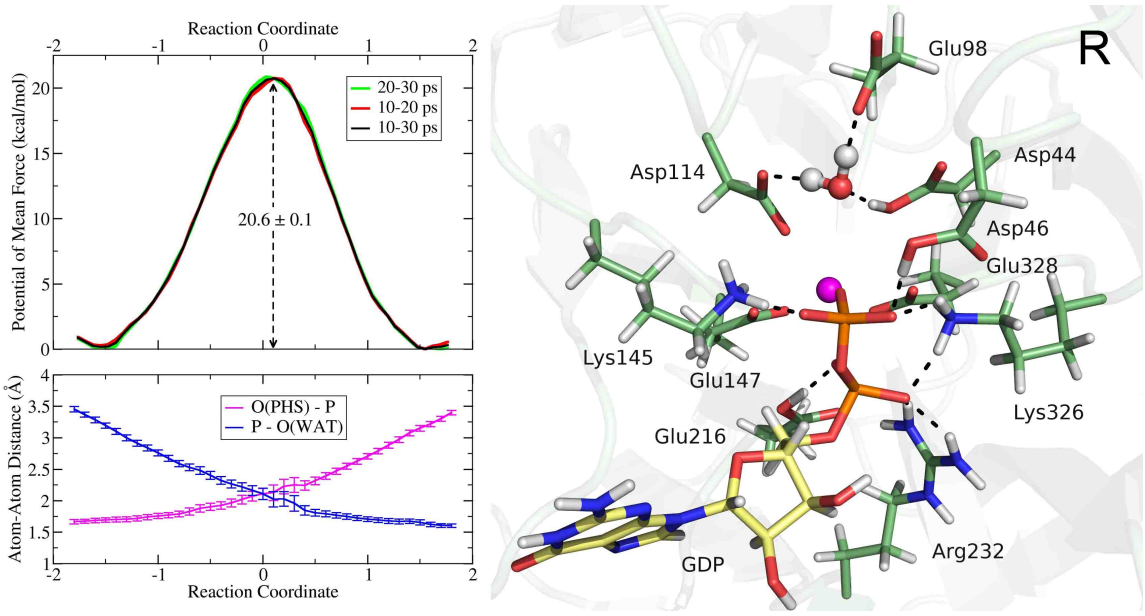

Figure S10. The free energy profile for the phosphoryl transfer reaction starting from an alternate protonation state (Asp114 is deprotonated). The bottom plot shows distance averages and standard deviations for the two bonds in the *RC*, and the reactant state is depicted on the right. The barrier to phosphoryl transfer from this state is relatively reasonable, but the active site is only briefly stable during the molecular dynamics trajectory of this reactant state. Asp114 is drawn toward Lys145, which disrupts the orientation of the nucleophilic water.

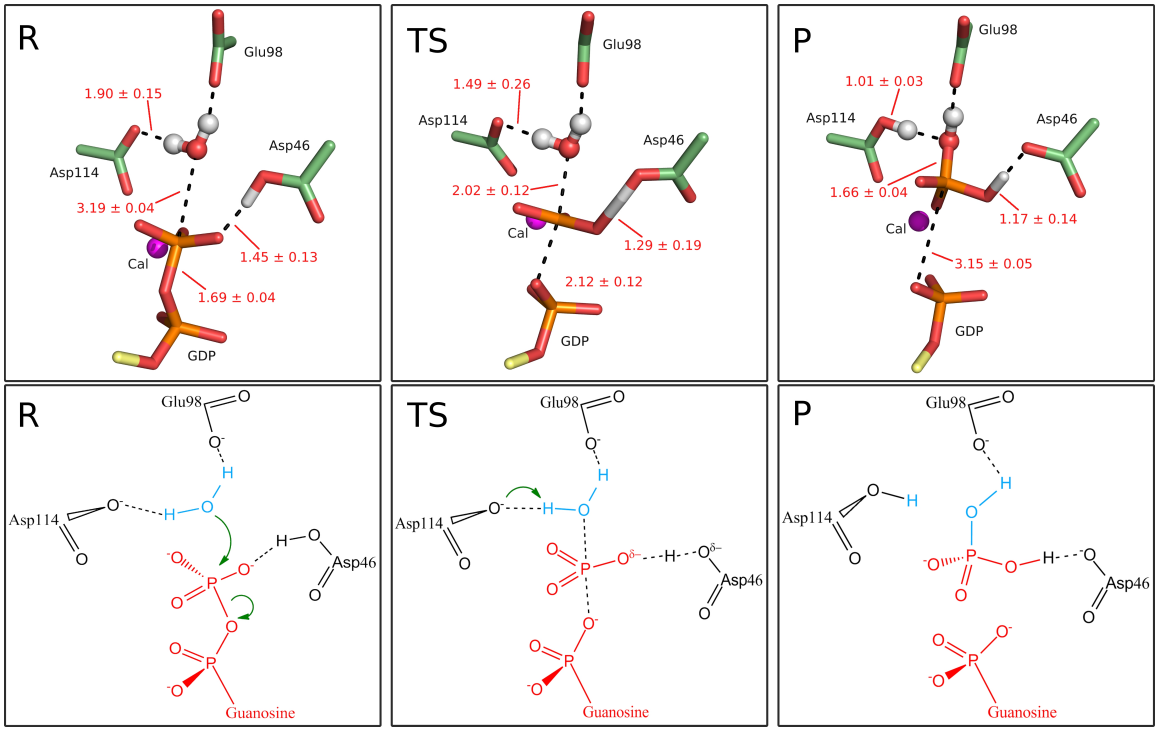

Figure S11. Line drawings and structures from the QM/MM-MD simulations for the reactant, transition state, and product for the alternate protonation state (Asp114 is deprotonated). Average distances and standard deviations for the bonds breaking from and forming to the phosphorous and for the proton transfers are shown in Å.

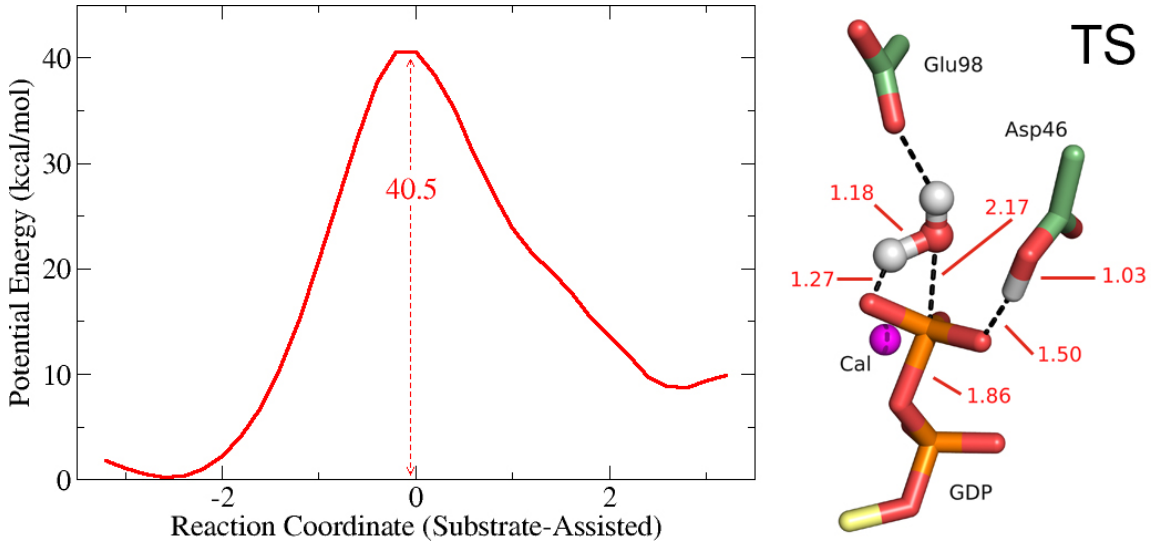

Figure S12. Potential energy profile and transition state structure for a substrate-assisted mechanism. The strained geometry of the simultaneous nucleophilic attack and substrate-assisted proton abstraction leads to a high activation energy for this mechanism.

Complete Citation for References 10, 13, 24, 40, 78, and 79:

(10) Gayle, R. B.; Maliszewski, C. R.; Gimpel, S. D.; Schoenborn, M. A.; Caspary, R. G.; Richards, C.; Brasel, K.; Price, V.; Drosopoulos, J. H.; Islam, N.; Alyonycheva, T. N.; Broekman, M. J.; Marcus, A. J. *The Journal of clinical investigation* **1998**, *101*, 1851.

(13) Finn, R. D.; Mistry, J.; Tate, J.; Coggill, P.; Heger, A.; Pollington, J. E.; Gavin, O. L.; Gunasekaran, P.; Ceric, G.; Forslund, K.; Holm, L.; Sonnhammer, E. L. L.; Eddy, S. R.; Bateman, A. *Nucleic Acids Res.* **2010**, *38*, D211.

(24) Case, D. A.; Darden, T. A.; Cheatham, T. E.; Simmerling, C. L.; Wang, J.; Duke, R. E.; Luo, R.; Crowley, M.; Walker, R. C.; Zhang, W.; Merz, K. M.; Wang, B.; Hayik, S.; Roitberg, A.; Seabra, G.; Kolossvary, I.; Wong, K. F.; Paesani, F.; Vanicek, J.; Wu, X.; Brozell, S. R.; Steinkuhler, T.; Gohlke, H.; Yang, L.; Tan, C.; Mongan, J.; Hornak, V.; Cui, G.; Mathews, D. H.; Seetin, M. G.; Sagui, C.; Babin, V.; Kollman, P. A. *AMBER 10*, University of California: San Francisco.

(40) Shao, Y.; Molnar, L. F.; Jung, Y.; Kussmann J., O. C., Brown S. T., Gilbert A. T., Slipchenko L. V., Levchenko S. V., O'Neill D. P., DiStasio R. A., Lochan R. C., Wang T., Beran G. J., Besley N. A., Herbert J. M., Lin C. Y., Van Voorhis T., Chien S. H., Sodt A., Steele R. P., Rassolov V. A., Maslen P. E., Korambath P. P., Adamson R. D., Austin B., Baker J., Byrd E. F., Dachsel H., Doerksen R. J., Dreuw A., Dunietz B. D., Dutoi A. D., Furlani T. R., Gwaltney S. R., Heyden A., Hirata S., Hsu C. P., Kedziora G., Khalliulin R. Z., Klunzinger P., Lee A. M., Lee M. S., Liang W., Lotan I., Nair N., Peters B., Proynov E.I., Pieniazek P.A., Rhee Y.M., Ritchie J., Rosta E., Sherrill C.D., Simmonett A.C., Subotnik J.E., Woodcock H.L., Zhang W., Bell A.T., Chakraborty A. K., Chipman D. M., Keil F. J., Warshel A., Hehre W. J., Schaefer H. F., Kong J., Krylov A. I., Gill P. M., and Head-Gordon M. *Q-Chem,* , version 3.0; Q.

(78) Huber, C.; Oules, B.; Bertoli, M.; Chami, M.; Fradin, M.; Alanay, Y.; Al-Gazali, L. I.; Ausems, M. G.; Bitoun, P.; Cavalcanti, D. P.; Krebs, A.; Le Merrer, M.; Mortier, G.; Shafeghati, Y.; Superti-Furga, A.; Robertson, S. P.; Le Goff, C.; Muda, A. O.; Paterlini-Brechot, P.; Munnich, A.; Cormier-Daire, V. *Am. J. Hum. Genet.* **2009**, *85*, 706.

(79) Gerhardt, J.; Steinbrech, C.; Buchi, O.; Behnke, S.; Bohnert, A.; Fritzsche, F.; Liewen, H.; Stenner, F.; Wild, P.; Hermanns, T.; Muntener, M.; Dietel, M.; Jung, K.; Stephan, C.; Kristiansen, G. *The American journal of pathology* **2011**, *178*, 1847.